

pubs.acs.org/NanoLett Letter

Defect Engineering of WO₃ by Rapid Flame Reduction for Efficient Photoelectrochemical Conversion of Methane into Liquid Oxygenates

Ho Kun Woo, Ankit Kumar Gautam, Jaxiry S. Barroso-Martínez, Arthur P. Baddorf, Kai Zhou, Yoon Young Choi, Jiajun He, Alexander V. Mironenko, Joaquín Rodríguez-López, and Lili Cai*



Cite This: Nano Lett. 2023, 23, 11493-11500



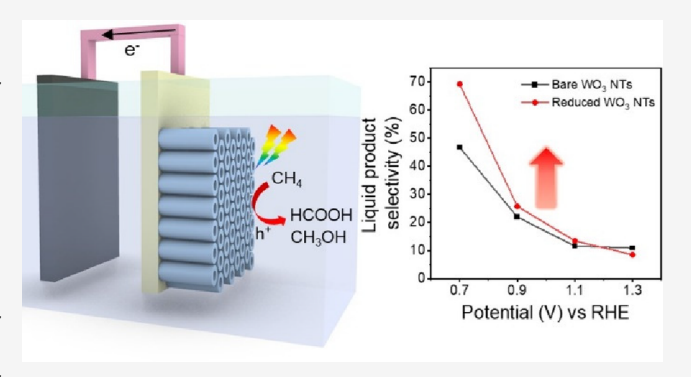
ACCESS I

III Metrics & More

Article Recommendations

s Supporting Information

ABSTRACT: Photoelectrochemical (PEC) conversion is a promising way to use methane (CH₄) as a chemical building block without harsh conditions. However, the PEC conversion of CH₄ to value-added chemicals remains challenging due to the thermodynamically favorable overoxidation of CH₄. Here, we report WO₃ nanotube (NT) photoelectrocatalysts for PEC CH₄ conversion with high liquid product selectivity through defect engineering. By tuning the flame reduction treatment, we carefully controlled the oxygen vacancies of WO₃ NTs. The optimally reduced WO₃ NTs suppressed overoxidation of CH₄ showing a high total C1 liquid selectivity of 69.4% and a production rate of 0.174 μ mol cm⁻² h⁻¹. Scanning electrochemical microscopy revealed that oxygen vacancies can restrain the production of



hydroxyl radicals, which, in excess, could further oxidize C1 intermediates to CO₂. Additionally, band diagram analysis and computational studies elucidated that oxygen vacancies thermodynamically suppress overoxidation. This work introduces a strategy for understanding and controlling the selectivity of photoelectrocatalysts for direct conversion of CH₄ to liquids.

KEYWORDS: methane oxidation, rapid flame reduction, defect engineering, photoelectrochemical conversion, tungsten trioxide

ethane (CH₄), the most prevalent component in natural gas, has drawn interest as an intermediate for the synthesis of energy-dense, transportable liquid fuels. Furthermore, CH₄ is a potent greenhouse gas accounting for 20% of global emissions, which needs to be reduced below its current level per the Paris Agreement. However, CH₄ has a symmetrically stable structure with a high C–H bonding energy, which impedes its effective conversion under ambient conditions. A common industrial practice of conversion of methane to a desired chemical feedstock involves steam methane reforming, which requires increased temperatures (>500 °C) and multistep processes. Thus, developing a direct and efficient method for transforming methane into a value-added chemical feedstock under mild conditions is imperative.

Catalytic conversion is a promising strategy for converting $\mathrm{CH_4}$ under ambient conditions by reducing the energy barrier for $\mathrm{C-H}$ activation. Several studies reported photochemical catalytic $\mathrm{CH_4}$ conversion with high selectivity. However, these approaches require costly oxidants such as $\mathrm{H_2O_2}$, which hinders the realization of an economically favorable $\mathrm{CH_4}$ conversion system. On the contrary, photoelectrochemical (PEC) oxidation using semiconductor electrodes is a potentially efficient approach for converting $\mathrm{CH_4}$ without additional oxidants. However, the PEC oxidation of $\mathrm{CH_4}$ in

water competes with oxygen evolution and the formation of hydroxyl radicals. The latter is considered one of the active species that can aid in the activation of CH₄ and formation of oxygenated products, while its excessive generation can lead to overoxidation to CO₂. Tungsten trioxide (WO₃) is a promising candidate as a PEC anode material for CH₄ conversion owing to its excellent hole mobility, desirable diffusion length, and appropriate valence band. ^{11–14} For example, facet-engineered WO₃ nanobar arrays have been reported to convert CH₄ to ethylene glycol with a high selectivity of 66% under solar illumination. ¹³ However, the PEC conversion of CH₄ to diverse carbon oxygenates remains a formidable challenge due to the thermodynamically favorable overoxidation to CO₂ or dominant oxygen evolution even at low potentials.

One of the most efficient ways to improve catalytic conversions is defect engineering of the catalysts, as it can

Received: August 18, 2023
Revised: December 4, 2023
Accepted: December 6, 2023
Published: December 7, 2023





influence the oxidation/reduction ability, catalytic site activity, and optical properties. $^{15-17}$ It was extensively researched employing a wide array of chemical and physical treatment methods for a variety of reactions ranging from water splitting to $\rm CO_2$ reduction. $^{18-21}$ In the realm of $\rm CH_4$ oxidation, the defect site can induce electron localization, which facilitates the activation of $\rm CH_4$ through $\rm C-H$ bond polarization. 22 Furthermore, defects can regulate the configuration of absorbed $\rm CH_4$ molecules on the surface of the catalyst, which is a critical step in converting $\rm CH_4$ into the desired products. 23 However, no studies have investigated the effect of defect engineering on PEC $\rm CH_4$ conversion.

Here, we report the rational design of WO₃ nanotubes (NTs) for PEC CH₄ conversion with high selectivity of C1 liquid products by defect engineering. WO₃ NTs were synthesized, and their oxygen vacancies were carefully tuned by a rapid flame reduction treatment. The optimized oxygen vacancies of WO₃ NTs successfully suppressed the overoxidation of CH₄ and achieved a high total C1 liquid product selectivity of 69.4% and a production rate of 0.174 μ mol cm⁻² h⁻¹, which surpassed the CO₂ selectivity of 28.6% and the production rate of 0.07 μ mol cm⁻² h⁻¹. We performed a full set of characterizations to investigate the origin of suppressing overoxidation in CH₄ conversion. With the aid of scanning electrochemical microscopy (SECM), we demonstrated that oxygen vacancies in WO3 NTs restrain the rate of generation of hydroxyl radicals that could lead to overoxidation to CO2 if it is present in excess. Additionally, oxygen vacancies increase the band energy level and decrease the electron affinity of catalyst surfaces, which thermodynamically suppresses overoxidation (Figure 1).

RESULTS AND DISCUSSION

The flame synthesis technique, which is fast, scalable, controllable, and cost-effective, was adopted for both the synthesis of WO_3 NTs and the control of oxygen vacancies. ^{24,25} In a typical WO_3 NT synthesis process, a seed

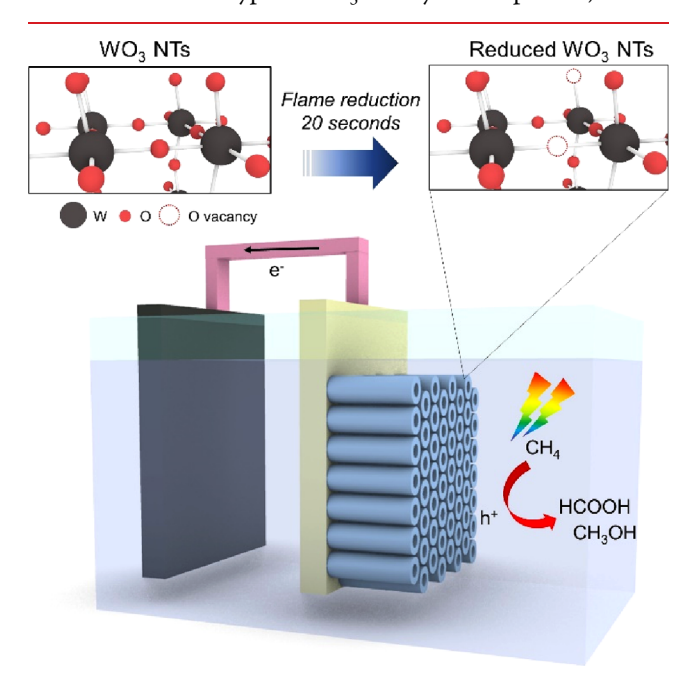


Figure 1. Schematic of the flame-reduced WO_3 NTs for PEC conversion of CH_4 .

layer was spin-coated on a FTO glass substrate. Then, crystalline substoichiometric $W_{18}O_{49}$ ($WO_{2.72}$) NTs were deposited by flame vapor deposition for 45 min (Figure S1). In this process, a substrate temperature of 520 °C and a flame equivalence ratio (ϕ) of 1.4 were employed to grow dense NTs. Next, through postannealing under 600 °C, crystalline WO₃ NTs were obtained. To control the oxygen vacancies, the as-prepared WO₃ NTs were treated with a premixed flat flame at a temperature of 900 °C. By controlling the fuel/air ratio, where fuel is slightly more abundant than air, we could create a reducing environment with the flame in which WO₃ NTs could be reduced with the formation of oxygen vacancies.

Panels a and b of Figure 2 show the side-view scanning electron microscopic (SEM) images of WO₃ NTs before and after reduction, respectively, in a flat flame for 20 s. The dense WO₃ NTs were vertically grown to a height of \sim 2.2 μ m. The top view of the SEM image clearly shows the hollow structures of the NTs (Figure S2). The reduced WO₃ NTs showed no significant difference in morphology compared to the bare WO₃ NTs in the top-view and side-view SEM images.

To investigate the crystallinity of WO₃ NT samples, X-ray diffraction (XRD) was performed (Figure 2c). Both the bare and reduced WO₃ NTs have a monoclinic WO₃ structure (ICSD No. 80055) and exhibit a growth direction along the [002] direction. Additionally, full widths at half-maximum and diffraction angles of each peak did not change noticeably during the short-duration, high-temperature flame reduction treatment, indicating no grain growth or phase alteration. Consistent with these results, transmission electron microscopy (TEM) analysis shows that the bare and reduced WO₃ NTs have the same *d* spacing of 0.38 nm along the [002] growth direction (Figure S3).

Next, to examine the effect of reduction on the chemical oxidation states, we conducted X-ray photoelectron spectroscopy (XPS). Figure 2d shows the W 4f XPS spectra with two major peaks. Each peak can be deconvoluted into two peaks, where the peaks at ~ 37.5 and ~ 35.4 eV represent W⁶⁺ while those at ~ 36.7 and ~ 34.6 eV correspond to W^{5+.26,27} After reduction, the percentage of the lower oxidation state W⁵⁺ increased from 1.8% to 5.2%, implying that the WO₃ NTs were successfully reduced, leading to the formation of oxygen vacancies.²⁸ Meanwhile, we observed negligible changes in the O 1s XPS spectra (Figure S4). This demonstrates that flame treatment has a minimal impact on the coordination polyhedron of oxygen surrounding tungsten, and no carbonates were formed after reduction.^{27,29} Furthermore, a hydroxyl peak (~532 eV) was not observed, which suggests that no H_xWO₃ phase was formed through flame reduction. Oxygen vacancy formation of reduced WO3 NTs was further confirmed by the light blue color, enhanced absorbance in the visible region of the ultraviolet-visible spectrum, and the distinct peak at g = 2.002 in the electron paramagnetic resonance spectrum (Figures S5 and S6).^{26,30}

Figure 3 shows the PEC performance of bare and reduced WO₃ NTs. Figure 3a illustrates a schematic of the experimental setup. PEC measurements were conducted in a gastight customized H-cell, where the anodic and catholic chambers were separated by a Nafion film. All reactions were studied at room temperature and atmospheric pressure in an acidic electrolyte (pH 2). Figure 3b shows linear sweep voltammetry (LSV) scans of the bare and reduced WO₃ NTs under 1 sun illumination. The magnified low-potential region, wider-range LSV scans to higher potentials, and cropped LSV scans are

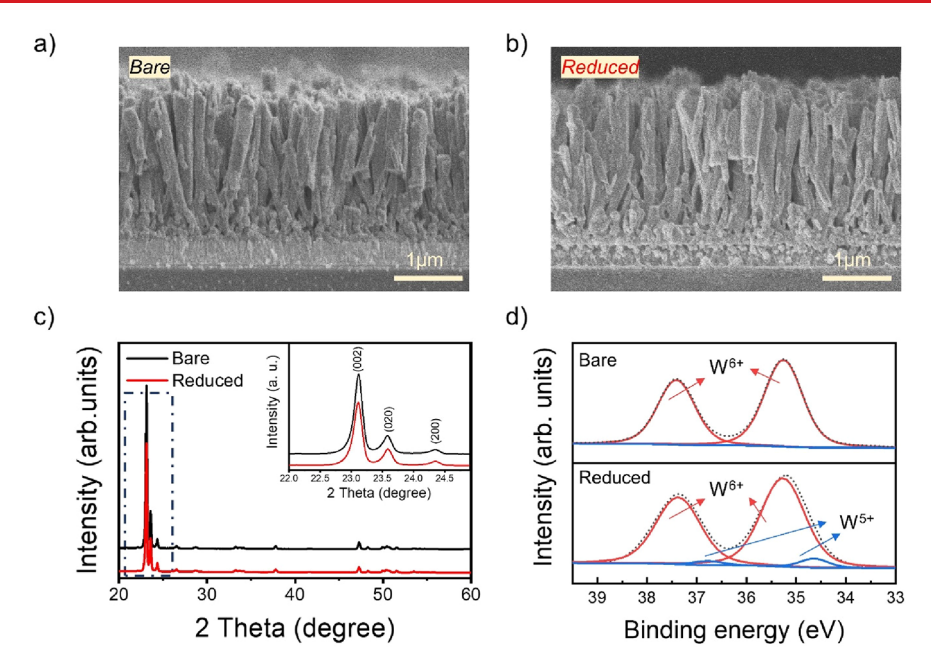


Figure 2. SEM images of (a) bare and (b) reduced WO₃ NTs. (c) XRD patterns and (d) XPS W 4f spectra of bare and reduced WO₃ NTs.

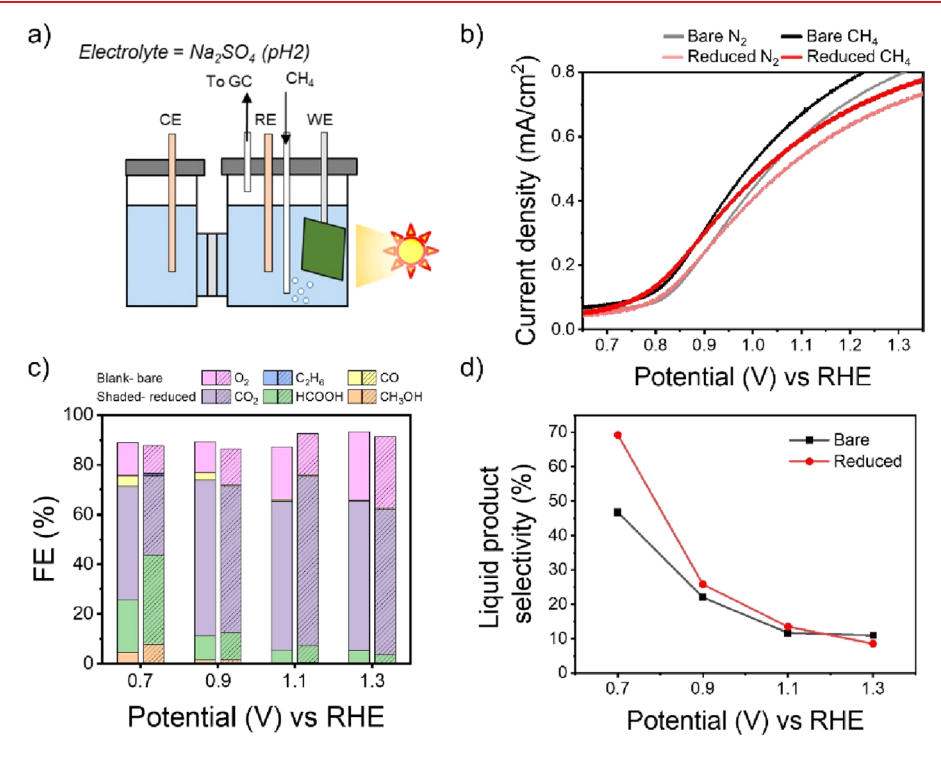


Figure 3. (a) Schematic of photoelectrolysis of CH₄. (b) LSV scans of bare and reduced WO₃ NTs under saturated nitrogen and CH₄ conditions with a scan rate of 25 mV/s. (c) FE for bare (blank) and reduced (shaded) WO₃ NTs electrodes. (d) Carbon selectivity of the liquid products produced in PEC CH₄ conversion.

shown in Figure S7. Nitrogen (N_2) or CH_4 gas was purged to form an N_2 - or CH_4 -saturated environment, respectively. Under CH_4 -saturated conditions, the LSV onset potential negatively shifts and shows a current value higher than that under N_2 -saturated conditions. This demonstrates that CH_4 oxidation is preferred over oxygen evolution on WO_3 NTs. Additionally, we performed electrochemical impedance spectroscopy to obtain Nyquist plots at 0.7 V versus the reference hydrogen electrode (RHE) (Figure S8). Both bare and reduced WO_3 NTs show a smaller semicircle under CH_4

conditions compared to N_2 conditions, indicating enhanced charge transfer at the $WO_3/electrolyte$ interface. This improvement could be attributed to the more facile reaction of photoholes with methane, which is consistent with the higher current in LSV scans under CH_4 conditions.

To further investigate the PEC CH_4 oxidation, photoelectrolysis at 0.7–1.3 V versus the RHE was conducted for 1.5 h (Figure S9). The faradaic efficiency (FE) of each component is summarized in Figure 3c, where the blank and shaded bars indicate the FE of bare and reduced WO₃ NTs, respectively. Nano Letters pubs.acs.org/NanoLett Letter

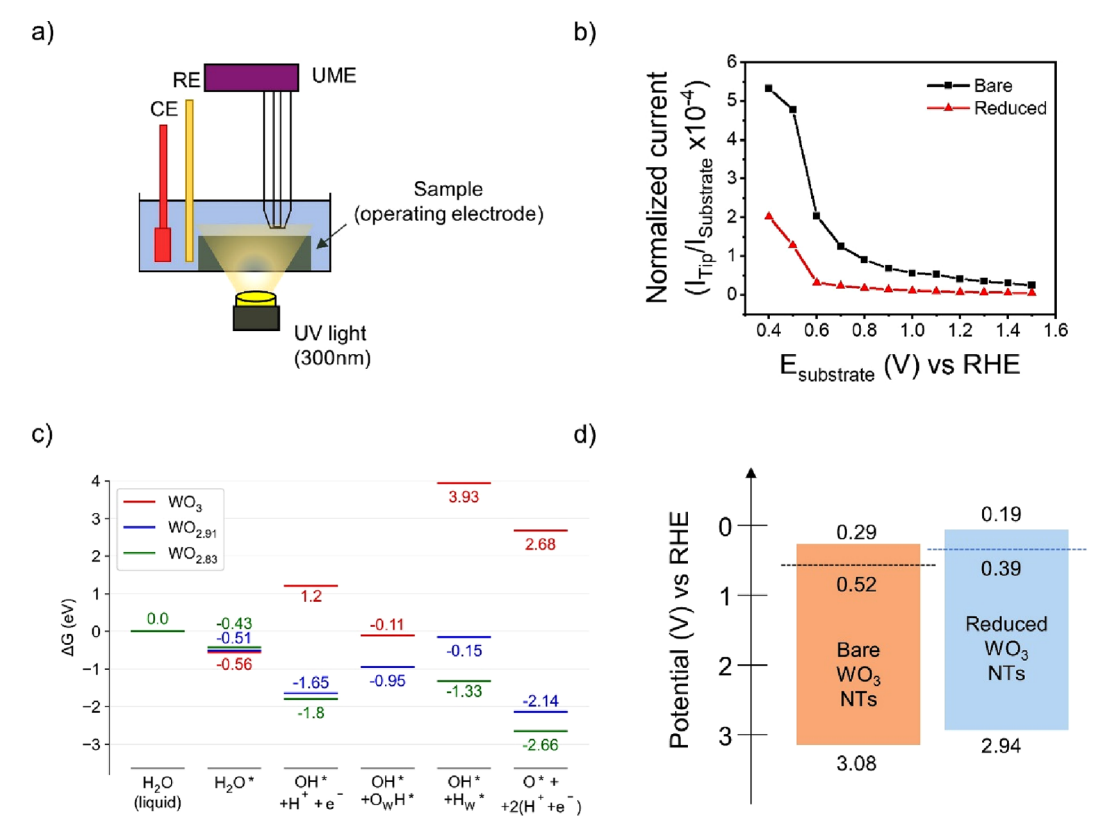


Figure 4. (a) Schematic of [DMPO-OH] • collection experiments by SECM. (b) Normalized tip collection current of [DMPO-OH] • from cyclic voltammograms recorded in a Au UME tip immersed $10 \, \mu m$ from a bare or reduced WO₃ NT substrate biased at different substrate potentials, in a solution containing $10 \, mM$ DMPO and Na₂SO₄ (pH 2). (c) Free energy diagram of water decomposition on the WO₃ (100) surface at pH 2 and a $U_{\rm RHE}$ of 0.7 V. (d) Schematic depicting the overall band diagrams of bare and reduced WO₃ NTs.

Similar to previously reported results, the most dominant reaction was the complete oxidation of CH₄ to CO₂. 11,31 However, at 0.7 V versus the RHE, reduced WO₃ NTs show a higher FE for liquid intermediate oxygenate species (CH₃OH and HCOOH) than for overoxidation species (CO₂ and CO). In particular, the HCOOH FE (35.8%) was higher than the CO₂ FE (32.1%). The selectivity of all liquid products at 0.7 V versus the RHE for reduced WO₃ NTs was 69.4%, while bare WO₃ NTs showed a value of only 45.3% (Figure 3d). The total liquid production rate (CH₃OH and HCOOH) was 0.174 μ mol cm⁻² h⁻¹, which was higher than that of bare WO₃ NTs $(0.132 \ \mu \text{mol cm}^{-2} \ \text{h}^{-1})$ even though bare WO₃ NTs showed a slightly higher photocurrent. To the best of our knowledge, such a high C1 liquid product selectivity from PEC CH4 conversion under mild conditions has never been reported (Table S1). In addition, the negligible difference in photocurrent density after 30 min and the FE of HCOOH after reaction for 4.5 h indicate the stability of reduced WO₃ NTs for long-term PEC CH₄ conversion (Figure S10). At 0.9 V versus the RHE, the reduced WO3 NTs had a higher FE of liquid products and a lower FE of overoxidation species, compared to those of bare WO₃ NTs. For potentials of >0.9 V versus the RHE, CO₂ accounted for the vast majority of products for bare and reduced WO3 NTs, as overoxidation to CO₂ is the most thermodynamically favorable reaction at high potentials. The CO₂ FE was higher for reduced samples than for bare WO3 NTs at 1.1 V versus the RHE, and it reached a similar value for both cases at 1.3 V versus the RHE. The production rate and selectivity of C1 liquid products decreased as the applied potential increased. The increased selectivity and

FE of liquid products at an even lower potential of 0.65 V versus the RHE also support the selectivity trends (Figure S11). We hypothesize that an increase in potential would accelerate the transfer of photogenerated carriers on the surface of WO₃ NTs, resulting in excess reactive intermediates, such as hydroxyl radical (\bullet OH) and other oxygen-containing radicals, which could expedite CH₄ overoxidation and oxygen evolution. Notably, trace amounts of H₂O₂ were detected only at the high potential of 1.3 V versus the RHE (Figure S12). No detectable amount of C1 oxygenates was found in the absence of an electrical bias or illumination (Figure S13).

Additionally, the flame reduction time was varied to control the amount of oxygen vacancies and to evaluate their effect on PEC CH₄ conversion (Figure S14). A 10 s reduction treatment resulted in a slightly higher photocurrent but a lower liquid selectivity compared to those of bare samples. The prolonged reduction time of >20 s led to a decrease in the photocurrent. Because excessive oxygen vacancies could act as recombination sites for photogenerated holes, the rates of production of C1 oxygenates under these conditions were much lower than that of the optimized reduction treatment time of 20 s. 32,33

According to previous studies, •OH as a strong oxidizing agent to activate methane can be produced by water photoelectrolysis. ^{9,34} To confirm the •OH generation in our PEC conversion process and study the effect of •OH with respect to PEC CH₄ conversion, we performed scanning electrochemical microscopy (SECM) experiments in the substrate-generation tip collection mode using a recently reported methodology. ³⁵ Here, the rate of generation of •OH at the operating electrodes was evaluated by using a lifetime-

extending spin trap, 5,5-dimethyl-1-pyrroline N-oxide (DMPO). Figure 4a shows the experimental configuration with back illumination following the SECM configuration reported elsewhere. DMPO-OH] \bullet collection experiments were performed with WO₃ NT substrates kept under illumination and biased to different potentials ($E_{\text{Substrate}}$) with a quiet time of 60 s, while cyclic voltammograms were recorded at 10 mV s⁻¹ using a Au ultramicroelectrode (UME) tip to collect the [DMPO-OH] \bullet species formed by the spin trapping reaction between DMPO and the \bullet OH produced during the photoelectrolysis of water at these electrodes. 13

Figure S15 shows the results of the [DMPO-OH]. collection experiments obtained when the bare and reduced WO₃ NT substrates were polarized at different potentials under dark and illumination conditions. As expected, when the catalytic surfaces were not irradiated, no [DMPO-OH]. collection current in the UME tip was detected (Figure S15a,b). Instead, when the WO₃ surfaces were kept irradiated and biased at different potentials (Figure S15c,d), the UME tip response showed an increasing current trend as the substrate current increased. The normalized current of the UME tip with the substrate current is shown in Figure 4b and Figure S16. This quantitative comparison shows that the [DMPO-OH]• collection from bare WO₃ NTs was higher than that of reduced WO₃ NTs, demonstrating that bare WO₃ NTs afford more •OH photoelectrochemical production as the substrate potential increases.

To further investigate the formation of •OH on WO₃ surfaces, we carried out ground-state DFT calculations of water decomposition on three representative WO3 surface facets, i.e., (100), (010), and (001), which correspond to the side and top facets of WO₃ NTs (Figure S17). We found surface OH* and O* formation to be exergonic with respect to liquid water and H⁺/e⁻ pairs on reduced surfaces in the absence of ultraviolet (UV) light, with Gibbs free energies of formation reaching -1.8 and -2.66 eV, respectively, on the WO_{2.83} (100) model surface (Figure 4c). Interestingly, all three facets of the reduced cases considered here exhibit greater OH_x^* (x = 0, 1, or 2) stabilization with an increasing degree of surface reduction (Figure 4c and Figures S18 and S19), while the (100) facet shows the greatest OH_x* stability on the surface. Curiously, the formation of O^* from OH^* is thermodynamically favorable and will become even more favorable at higher potentials, which may deplete the surface of OH*. This is consistent with the decreased level of •OH production (Figure 4b) and the reduced selectivity to liquid products at high potentials (Figure 3d).

On the bare WO₃ surface in the dark, H₂O dissociation is largely energetically unfavorable, consistent with the lack of experimentally observed •OH in the absence of UV light. As UV irradiation photoexcites WO₃ by at least the band gap value (2.85 eV from Figure S20), the formation of OH,* species would, in the first approximation, become more exergonic by the same value, if we assume a thermodynamic equilibrium among liquid H2O, photoexcited WO3, and chemisorbed OH_x^* in the ground state. Consequently, the states $OH^* + H^+ + e^-$ and $OH^* + O_wH^*$ (Figure 4c) would become thermodynamically accessible on bare WO₃ under UV light. In contrast to the reduced WO3 surface, on the bare surface the hydroxyl groups do not transform into O*, as the latter is highly unstable [2.68 eV (Figure 4c)], favoring ●OH formation. We hypothesize that the $OH^* + H^+ + e^-$ state gives rise to the current associated with •OH formation in the

SECM experiment, owing to the weak interaction of OH* with the surface in the ground state [1.20 eV (Figure 4c)] and thus its high reactivity. The spin density isosurface plotted in Figure S21 for the OH*/WO₃ (100) structure confirms the partial radical character of the OH* species, with an unpaired electron delocalized over several surface oxygen atoms. Radical formation mediated by the OH* + H+ + e- state on the bare surface is consistent with the potential dependence of the normalized tip collection current of [DMPO-OH] ● (Figure 4b). Indeed, less positive potentials destabilize this state, making OH* more reactive and explaining the rapid increase in the current observed at lower potentials on the bare surface. Overall, the reduced WO3 has greater OH* stability in comparison with the bare WO3 based on DFT calculations while having a lower rate of production of •OH in the electrolyte solution based on the previously discussed SECM results. As •OH radicals have a high oxidative reactivity, they could contribute to overoxidation to CO2. 38,39 In this regard, the reduced WO3 NTs, which produce fewer •OH radicals in the electrolyte, are less likely to fully oxidize intermediate oxygenates to CO₂ as observed in photoelectrolysis experiments.

In addition, the location of the valence band maximum (VBM) also plays an important role, as it thermodynamically determines the oxidation power. 40,41 The energy states of bare and reduced WO3 NTs were examined to further elucidate the mechanisms of suppressing overoxidation and increasing intermediate oxygenate production. The total energy-band diagrams were calculated through a combination of Mott-Schottky plots, Tauc plots, and UPS characterizations (Figure S22 and Figure 4d). The VBM of the bare WO₃ NTs was deeper than that of the reduced WO3 NTs. Therefore, the reduced WO₃ NTs thermodynamically generate less oxidation power. As a result, for the reduced WO₃ NTs, overoxidation of CH₄ was suppressed, and the production of intermediate oxygenates was promoted at low potentials. However, at high potentials, due to the high oxidation power from the electrical bias, regardless of the location of the VBM, both samples show overoxidation to CO2 as shown in the CH4 photoelectrolysis experiment results.

DFT calculations of electron affinity (EA) corroborated the aforementioned argument that the reduced surfaces possess less oxidation power. Two different EA calculation methods (Figure S23 and Tables S2 and S3) revealed that the bare surfaces possess greater EA values in comparison with the reduced surfaces and thus should exhibit a greater propensity for accepting electrons. The lower oxidizing power of the reduced states makes partial oxidation favorable over full oxidation to CO₂.

In summary, we realized PEC conversion of CH_4 at ambient conditions with a high C1 liquid product selectivity through defect engineering of catalysts. The optimized flame-reduced WO₃ NTs attained a high total liquid product selectivity of 69.4% and a production rate of 0.174 μ mol cm⁻² h⁻¹ while exhibiting a suppressed CO₂ production rate. Using SECM, we showed that the oxygen vacancies in the WO₃ NTs restrain the production of \bullet OH radicals, which are responsible for accelerating CH₄ overoxidation. Additionally, oxygen vacancies increase the band energy level of WO₃ NTs and decrease the electron affinity, making overoxidation thermodynamically unfavorable. We conclude that decreasing the oxidative power of photoelectrocatalysts is a key to increasing the rate

Nano Letters pubs.acs.org/NanoLett Letter

of production of intermediate oxygenates from PEC $\mathrm{CH_4}$ conversion.

ASSOCIATED CONTENT

5 Supporting Information

The Supporting Information is available free of charge at https://pubs.acs.org/doi/10.1021/acs.nanolett.3c03131.

Experimental methods and computational details; digital photographs, SEM, HR-TEM, XPS, and UV—vis data and wider-range LSV scans of bare and reduced WO₃ NTs; ¹H NMR spectra and H₂O₂ detection after photoelectrolysis; DMPO—OH collection experiment, including the tip and substrate current; band diagram analysis; free energy diagram of water decomposition on various WO₃ facets; and electroaffinity calculation (PDF)

AUTHOR INFORMATION

Corresponding Author

Lili Cai — Department of Mechanical Science and Engineering and Materials Research Laboratory, University of Illinois Urbana-Champaign, Urbana, Illinois 61801, United States; orcid.org/0000-0003-1222-248X; Email: lilicai@illinois.edu

Authors

Ho Kun Woo – Department of Mechanical Science and Engineering, University of Illinois Urbana-Champaign, Urbana, Illinois 61801, United States; orcid.org/0000-0001-5904-8082

Ankit Kumar Gautam – Department of Chemical and Biomolecular Engineering, University of Illinois Urbana-Champaign, Urbana, Illinois 61801, United States

Jaxiry S. Barroso-Martínez – Department of Chemistry, University of Illinois Urbana-Champaign, Urbana, Illinois 61801, United States

Arthur P. Baddorf – Center for Nanophase Materials Sciences, Oak Ridge National Laboratory, Oak Ridge, Tennessee 37831, United States

Kai Zhou – Department of Mechanical Science and Engineering, University of Illinois Urbana-Champaign, Urbana, Illinois 61801, United States; orcid.org/0000-0003-4653-6436

Yoon Young Choi – Department of Mechanical Science and Engineering, University of Illinois Urbana-Champaign, Urbana, Illinois 61801, United States

Jiajun He — Department of Mechanical Science and Engineering, University of Illinois Urbana-Champaign, Urbana, Illinois 61801, United States

Alexander V. Mironenko – Department of Chemical and Biomolecular Engineering, University of Illinois Urbana-Champaign, Urbana, Illinois 61801, United States;
orcid.org/0000-0001-7490-5038

Joaquín Rodríguez-López — Department of Chemistry, Beckman Institute for Advanced Science and Technology, and Materials Research Laboratory, University of Illinois Urbana-Champaign, Urbana, Illinois 61801, United States; orcid.org/0000-0003-4346-4668

Complete contact information is available at: https://pubs.acs.org/10.1021/acs.nanolett.3c03131

Author Contributions

H.K.W. and L.C. conceived the idea. H.K.W. carried out the material synthesis and performed SEM, TEM, UV—vis, Mott—Schottky, and photoelectrolysis of methane. A.K.G. and A.V.M. designed, conducted, and interpreted DFT calculations. J.S.B.-M. and J.R.-L. performed SECM experiments. A.P.B. carried out UPS. K.Z. carried out XRD. Y.Y.C. helped with data analysis. J.H. assisted in building the PEC measurement setup. H.K.W. and L.C. wrote the manuscript with input from all of the authors. All authors discussed the results and revised the paper.

Notes

The authors declare no competing financial interest.

ACKNOWLEDGMENTS

This work was supported by the donors of the ACS Petroleum Research Fund (PRF) under Doctoral New Investigator Grant 65618-DNI5. L.C. served as Principal Investigator on ACS PRF 65618-DNI5 that provided support for H.K.W. This research was also financially supported by the startup fund from University of Illinois at Urbana-Champaign, J.S.B.-M. and J.R.-L. acknowledge support from the National Science Foundation under CHE Grant 2004054. H.K.W. acknowledges support from the TechnipFMC Fellowship. ¹H NMR was carried out in the School of Chemical Sciences NMR Lab at the University of Illinois at Urbana-Champaign. The authors acknowledge Dr. D. L. Olson of the University of Illinois at Urbana-Champaign for the NMR analysis. Major funding for the Bruker EMXPlus instrument was provided by National Science Foundation Grant 1726244 (2017) to the School of Chemical Sciences EPR lab at the University of Illinois at Urbana-Champaign. TEM, XRD, SEM, UV-vis, and XPS were conducted in the Materials Research Laboratory at the University of Illinois at Urbana-Champaign. UV photoemission spectroscopy research was conducted as part of a user project at the Center for Nanophase Materials Sciences (CNMS), which is a U.S. Department of Energy Office of Science User Facility at Oak Ridge National Laboratory.

REFERENCES

- (1) Song, H.; Meng, X.; Wang, Z.-j.; Liu, H.; Ye, J. Solar-Energy-Mediated Methane Conversion. *Joule* **2019**, *3*, 1606–1636.
- (2) Mortensen, R. L.; Noack, H. D.; Pedersen, K.; Mossin, S.; Mielby, J. Recent Advances in Complete Methane Oxidation Using Zeolite-Supported Metal Nanoparticle Catalysts. *ChemCatChem* **2022**, *14*, No. e202101924.
- (3) Nisbet, E. G.; Fisher, R. E.; Lowry, D.; France, J. L.; Allen, G.; Bakkaloglu, S.; Broderick, T. J.; Cain, M.; Coleman, M.; Fernandez, J.; Forster, G.; Griffiths, P. T.; Iverach, C. P.; Kelly, B. F. J.; Manning, M. R.; Nisbet-Jones, P. B. R.; Pyle, J. A.; Townsend-Small, A.; al-Shalaan, A.; Warwick, N.; Zazzeri, G. Methane Mitigation: Methods to Reduce Emissions, on the Path to the Paris Agreement. *Rev. Geophys.* 2020, 58, No. e2019RG000675.
- (4) Liu, Z.; Huang, E.; Orozco, I.; Liao, W.; Palomino, R. M.; Rui, N.; Duchoň, T.; Nemšák, S.; Grinter, D. C.; Mahapatra, M.; Liu, P.; Rodriguez, J. A.; Senanayake, S. D. Water-Promoted Interfacial Pathways in Methane Oxidation to Methanol on a CeO₂-Cu₂O Catalyst. *Science* **2020**, *368*, 513–517.
- (5) Laosiripojana, N.; Assabumrungrat, S. Catalytic Steam Reforming of Methane, Methanol, and Ethanol over Ni/YSZ: The Possible Use of These Fuels in Internal Reforming SOFC. *J. Power Sources* **2007**, *163*, 943–951.
- (6) Szécsényi, Á.; Li, G.; Gascon, J.; Pidko, E. A. Mechanistic Complexity of Methane Oxidation with $\rm H_2O_2$ by Single-Site Fe/ZSM-5 Catalyst. ACS Catal. **2018**, 8, 7961–7972.

- (7) Serra-Maia, R.; Michel, F. M.; Kang, Y.; Stach, E. A. Decomposition of Hydrogen Peroxide Catalyzed by AuPd Nanocatalysts during Methane Oxidation to Methanol. *ACS Catal.* **2020**, *10*, 5115–5123.
- (8) Xie, J.; Jin, R.; Li, A.; Bi, Y.; Ruan, Q.; Deng, Y.; Zhang, Y.; Yao, S.; Sankar, G.; Ma, D.; Tang, J. Highly Selective Oxidation of Methane to Methanol at Ambient Conditions by Titanium Dioxide-Supported Iron Species. *Nat. Catal.* **2018**, *1*, 889–896.
- (9) Cheng, F.; Lin, G.; Hu, X.; Xi, S.; Xie, K. Porous Single-Crystalline Titanium Dioxide at 2 Cm Scale Delivering Enhanced Photoelectrochemical Performance. *Nat. Commun.* **2022**, *13*, 6677.
- (10) Narsimhan, K.; Iyoki, K.; Dinh, K.; Román-Leshkov, Y. Catalytic Oxidation of Methane into Methanol over Copper-Exchanged Zeolites with Oxygen at Low Temperature. *ACS Cent. Sci.* **2016**, *2*, 424–429.
- (11) Amano, F.; Shintani, A.; Tsurui, K.; Mukohara, H.; Ohno, T.; Takenaka, S. Photoelectrochemical Homocoupling of Methane under Blue Light Irradiation. *ACS Energy Lett.* **2019**, *4*, 502–507.
- (12) Rao, P. M.; Cai, L.; Liu, C.; Cho, I. S.; Lee, C. H.; Weisse, J. M.; Yang, P.; Zheng, X. Simultaneously Efficient Light Absorption and Charge Separation in WO₃/BiVO₄ Core/Shell Nanowire Photoanode for Photoelectrochemical Water Oxidation. *Nano Lett.* **2014**, *14*, 1099–1105.
- (13) Ma, J.; Mao, K.; Low, J.; Wang, Z.; Xi, D.; Zhang, W.; Ju, H.; Qi, Z.; Long, R.; Wu, X.; Song, L.; Xiong, Y. Efficient Photoelectrochemical Conversion of Methane into Ethylene Glycol by WO₃ Nanobar Arrays. *Angew. Chem., Int. Ed.* **2021**, *60*, 9357–9361.
- (14) Wang, Y.; Tian, W.; Chen, C.; Xu, W.; Li, L. Tungsten Trioxide Nanostructures for Photoelectrochemical Water Splitting: Material Engineering and Charge Carrier Dynamic Manipulation. *Adv. Funct. Mater.* **2019**, 29, 1809036.
- (15) Li, W.; Wang, D.; Zhang, Y.; Tao, L.; Wang, T.; Zou, Y.; Wang, Y.; Chen, R.; Wang, S. Defect Engineering for Fuel-Cell Electrocatalysts. *Adv. Mater.* **2020**, 32, 1907879.
- (16) Steenhaut, T.; Grégoire, N.; Barozzino-Consiglio, G.; Filinchuk, Y.; Hermans, S. Mechanochemical Defect Engineering of HKUST-1 and Impact of the Resulting Defects on Carbon Dioxide Sorption and Catalytic Cyclopropanation. *RSC Adv.* **2020**, *10*, 19822–19831.
- (17) Qi, Y.; Song, L.; Ouyang, S.; Liang, X.; Ning, S.; Zhang, Q. Q.; Ye, J. Photoinduced Defect Engineering: Enhanced Photothermal Catalytic Performance of 2D Black In₂O_{3-x} Nanosheets with Bifunctional Oxygen Vacancies. *Adv. Mater.* **2020**, *32*, 1903915.
- (18) Tan, R.; Sivanantham, A.; Jansi Rani, B.; Jeong, Y. J.; Cho, I. S. Recent Advances in Surface Regulation and Engineering Strategies of Photoelectrodes toward Enhanced Photoelectrochemical Water Splitting. *Coord. Chem. Rev.* **2023**, 494, 215362.
- (19) Shao, C.; Malik, A. S.; Han, J.; Li, D.; Dupuis, M.; Zong, X.; Li, C. Oxygen Vacancy Engineering with Flame Heating Approach towards Enhanced Photoelectrochemical Water Oxidation on WO3 Photoanode. *Nano Energy* **2020**, *77*, 105190.
- (20) Chen, H.; Handoko, A. D.; Wang, T.; Qu, J.; Xiao, J.; Liu, X.; Legut, D.; Wei Seh, Z.; Zhang, Q. Defect-Enhanced CO2 Reduction Catalytic Performance in O-Terminated MXenes. *ChemSusChem* **2020**, *13* (21), 5690–5698.
- (21) Tan, R.; Jeong, Y. J.; Li, Q.; Kang, M.; Cho, I. S. Defect-Rich Spinel Ferrites with Improved Charge Collection Properties for Efficient Solar Water Splitting. J. Adv. Ceram. 2023, 12 (3), 612–624.
- (22) Zhou, Y.; Zhang, L.; Wang, W. Direct Functionalization of Methane into Ethanol over Copper Modified Polymeric Carbon Nitride via Photocatalysis. *Nat. Commun.* **2019**, *10*, 506.
- (23) Chen, Z.; Wu, S.; Ma, J.; Mine, S.; Toyao, T.; Matsuoka, M.; Wang, L.; Zhang, J. Non-Oxidative Coupling of Methane: N-Type Doping of Niobium Single Atoms in TiO₂-SiO₂ Induces Electron Localization. *Angew. Chem., Int. Ed.* **2021**, *60*, 11901–11909.
- (24) Cho, I. S.; Logar, M.; Lee, C. H.; Cai, L.; Prinz, F. B.; Zheng, X. Rapid and Controllable Flame Reduction of TiO₂ Nanowires for Enhanced Solar Water-Splitting. *Nano Lett.* **2014**, *14*, 24–31.

- (25) Ding, J. R.; Kim, K. S. Rapid Growth of Vertically Aligned Tungsten Oxide Nanostructures by Flame Vapor Deposition Process. *Chem. Eng. J.* **2016**, 300, 47–53.
- (26) Kalanur, S. S.; Yoo, I. H.; Cho, I. S.; Seo, H. Effect of Oxygen Vacancies on the Band Edge Properties of WO₃ Producing Enhanced Photocurrents. *Electrochim. Acta* **2019**, 296, 517–527.
- (27) Li, W.; Da, P.; Zhang, Y.; Wang, Y.; Lin, X.; Gong, X.; Zheng, G. WO₃ Nanoflakes for Enhanced Photoelectrochemical Conversion. *ACS Nano* **2014**, *8*, 11770–11777.
- (28) Sun, M.; Gao, R. T.; He, J.; Liu, X.; Nakajima, T.; Zhang, X.; Wang, L. Photo-Driven Oxygen Vacancies Extends Charge Carrier Lifetime for Efficient Solar Water Splitting. *Angew. Chem., Int. Ed.* **2021**, *60*, 17601–17607.
- (29) Shao, C.; Malik, A. S.; Han, J.; Li, D.; Dupuis, M.; Zong, X.; Li, C. Oxygen Vacancy Engineering with Flame Heating Approach towards Enhanced Photoelectrochemical Water Oxidation on WO3 Photoanode. *Nano Energy* **2020**, *77*, 105190.
- (30) Lei, B.; Cui, W.; Chen, P.; Chen, L.; Li, J.; Dong, F. C-Doping Induced Oxygen-Vacancy in WO3Nanosheets for CO2Activation and Photoreduction. ACS Catal. 2022, 12 (15), 9670–9678.
- (31) Kadosh, Y.; Korin, E.; Bettelheim, A. Room-Temperature Conversion of the Photoelectrochemical Oxidation of Methane into Electricity at Nanostructured TiO2. *Sustain. Energy Fuels* **2021**, *5*, 127–134.
- (32) Kato, K.; Uemura, Y.; Asakura, K.; Yamakata, A. Role of Oxygen Vacancy in the Photocarrier Dynamics of WO₃ Photocatalysts: The Case of Recombination Centers. *J. Phys. Chem. C* **2022**, *126*, 9257–9263.
- (33) Corby, S.; Francàs, L.; Kafizas, A.; Durrant, J. R. Determining the Role of Oxygen Vacancies in the Photoelectrocatalytic Performance of WO₃ for Water Oxidation. *Chem. Sci.* **2020**, *11*, 2907–2914.
- (34) Luo, L.; Wang, Z. J.; Xiang, X.; Yan, D.; Ye, J. Selective Activation of Benzyl Alcohol Coupled with Photoelectrochemical Water Oxidation via a Radical Relay Strategy. *ACS Catal.* **2020**, *10*, 4906–4913.
- (35) Barroso-Martínez, J. S.; Romo, A. I. B.; Pudar, S.; Putnam, S. T.; Bustos, E.; Rodríguez-López, J. Real-Time Detection of Hydroxyl Radical Generated at Operating Electrodes via Redox-Active Adduct Formation Using Scanning Electrochemical Microscopy. *J. Am. Chem. Soc.* 2022, 144, 18896–18907.
- (36) Zhou, X.; Gossage, Z. T.; Simpson, B. H.; Hui, J.; Barton, Z. J.; Rodríguez-López, J. Electrochemical Imaging of Photoanodic Water Oxidation Enhancements on TiO2 Thin Films Modified by Subsurface Aluminum Nanodimers. ACS Nano 2016, 10, 9346–9352.
- (37) Krumov, M. R.; Simpson, B. H.; Counihan, M. J.; Rodríguez-López, J. In Situ Quantification of Surface Intermediates and Correlation to Discharge Products on Hematite Photoanodes Using a Combined Scanning Electrochemical Microscopy Approach. *Anal. Chem.* **2018**, *90*, 3050–3057.
- (38) Xie, J.; Jin, R.; Li, A.; Bi, Y.; Ruan, Q.; Deng, Y.; Zhang, Y.; Yao, S.; Sankar, G.; Ma, D.; Tang, J. Highly Selective Oxidation of Methane to Methanol at Ambient Conditions by Titanium Dioxide-Supported Iron Species. *Nat. Catal.* **2018**, *1*, 889.
- (39) Wang, S.; Rong, M.; Li, H.; Xu, T.; Bu, Y.; Chen, L.; Chen, X.; Yu, Z. P.; Zhu, X.; Lu, Z.; Zhou, H. Unveiling Mechanism of Organic Photogenerator for Hydroxyl Radicals Generation by Molecular Modulation. *Small* **2022**, *18*, 2104857.
- (40) Savateev, A.; Ghosh, I.; König, B.; Antonietti, M. Photoredoxkatalytische Organische Umwandlungen an Heterogenen Kohlenstoffnitriden. *Angew. Chem., Int. Ed.* **2018**, *130*, 16164–16176.
- (41) Wei, Z.; Wang, W.; Li, W.; Bai, X.; Zhao, J.; Tse, E. C. M.; Phillips, D. L.; Zhu, Y. Steering Electron-Hole Migration Pathways Using Oxygen Vacancies in Tungsten Oxides to Enhance Their Photocatalytic Oxygen Evolution Performance. *Angew. Chem., Int. Ed.* **2021**, *60*, 8236–8242.

Nano Letters pubs.acs.org/NanoLett Letter

■ NOTE ADDED AFTER ASAP PUBLICATION

This Letter was published ASAP on December 7, 2023. Minor changes have been made throughout and the corrected version was reposted on December 8, 2023.